Crystal Structure of the Complex between VEGF and a Receptor-Blocking Peptide‡

Christian Wiesmann,§ Hans W. Christinger,§ Andrea G. Cochran,§ Brian C. Cunningham,§,|| Wayne J. Fairbrother,§ Christopher J. Keenan,§ Gloria Meng,⊥ and Abraham M. de Vos*,§

Departments of Protein Engineering and BioAnalytical Technology, Genentech, Inc., 1 DNA Way, South San Francisco, California 94080

Received August 11, 1998; Revised Manuscript Received October 20, 1998

ABSTRACT: Vascular endothelial growth factor (VEGF) is a specific and potent angiogenic factor and, therefore, a prime therapeutic target for the development of antagonists for the treatment of cancer. As a first step toward this goal, phage display was used to generate peptides that bind to the receptor-binding domain (residues 8−109) of VEGF and compete with receptor [Fairbrother, W. J., Christinger, H. W., Cochran, A. G., Fuh, G., Keenan, C. J., Quan, C., Shriver, S. K., Tom, J. Y. K., Wells, J. A., and Cunningham, B. C. (1999) *Biochemistry 38*, 17754−17764]. The crystal structure of VEGF in complex with one of these peptides was solved and refined to a resolution of 1.9 Å. The 20-mer peptide is unstructured in solution and adopts a largely extended conformation when bound to VEGF. Residues 3−8 form a β-strand which pairs with strand β6 of VEGF via six hydrogen bonds. The C-terminal four residues of the peptide point away from the growth factor, consistent with NMR data indicating that these residues are flexible in the complex in solution. In contrast, shortening the N-terminus of the peptide leads to decreased binding affinities. Truncation studies show that the peptide can be reduced to 14 residues with only moderate effect on binding affinity. However, because of the extended conformation and the scarcity of specific side-chain interactions with VEGF, the peptide is not a promising lead for small-molecule development. The interface between the peptide and VEGF contains a subset of the residues recognized by a neutralizing Fab fragment and overlaps partially with the binding site for the Flt-1 receptor. The location of the peptide-binding site and the hydrophilic character of the interactions with VEGF resemble more the binding mode of the Fab fragment than that of the receptor.

Vascular endothelial growth factor (VEGF)[1] is a highly specific mitogen for endothelial cells and has a pivotal function in the regulation of vasculogenesis and angiogenesis (for a review, see ref *1*). At the molecular level, VEGF acts by binding to Flt-1 (fms-like tyrosine kinase) and KDR (kinase domain receptor). These receptor tyrosine kinases have seven Ig-like domains in their extracellular portion and are uniquely expressed on endothelial cells (*2*). VEGF also plays an important role in certain pathogenic states with raised levels of blood vessel formation, such as diabetic retinopathy and cancer (*3*, *4*); thus, antagonists that prevent receptor binding by VEGF may represent attractive therapeutics for the treatment of such diseases. This concept gained support when a neutralizing murine anti-VEGF antibody was shown to inhibit tumor growth in vivo (*5*); recently, a humanized version of this antibody was developed for testing in clinical trials (*6*, *7*).

Structure-based design of small-molecule VEGF antagonists depends on detailed structural and functional characterization of VEGF−receptor interactions. The high-resolution crystal structure of the receptor-binding domain of VEGF ($VEGF_{8-109}$) (*8*, *9*) showed that it belongs to the family of dimeric, cystine knot containing growth factors (for a review, see ref *10*). Each monomer contains three 2-stranded β-sheets and a short α-helix near the N-terminus. The strands carry the cystine knot motif at one end and a small hydrophobic core at the other. In forming the dimer, the monomers are arranged in an antiparallel, side-by-side fashion and are covalently linked by two disulfide bridges. Critical residues for KDR and Flt-1 binding were identified by mutagenesis studies (*9*, *11*). These studies, together with the crystal structure of the complex between VEGF and domain 2 of the Flt-1 receptor (*12*), showed that the receptor-binding face of VEGF covers the "pole" of the molecule and consists of residues contributed by both subunits of the dimer. Determination of the crystal structure of the complex with the Fab fragment of the humanized antibody revealed that the mechanism of action of the antibody is a partial blocking of the receptor-binding site, with the principal interactions at the periphery of this site (*13*).

The information available to date suggests that direct, structure-based design of small-molecule inhibitors would be unlikely to succeed. However, the development of small-molecule drug candidates based on structural information from small, constrained peptides has proven remarkably successful (*14*−*17*). As a first step toward generating such peptides, we have used naive peptide phage display tech-

‡ The coordinates have been deposited with the Brookhaven Protein Data Bank for immediate release, accession code 1vpp.

* To whom correspondence should be addressed. Phone: 650-225-2523. Fax: 650-225-3734. E-mail: devos@gene.com.

|| Present address: Sunesis Pharmaceuticals, Inc., 3696 Haven Avenue, Suite C, Redwood City, CA 94063.

⊥ Department of BioAnalytical Technology.

§ Department of Protein Engineering.

[1] Abbreviations: VEGF, vascular endothelial growth factor; KDR, kinase domain receptor; Flt-1, *fms*-like tyrosine kinase; Ig, immunoglobulin; rms, root-mean-square.

10.1021/bi9819327 CCC: $15.00
Published on Web 12/04/1998

niques to identify disulfide-constrained 16−20-mer peptides that bind to VEGF and block the interaction with the VEGF receptors (*18*). Here, we describe the high-resolution cocrystal structure of one of these peptides, compare its binding mode to those of the Flt-1 receptor and the antibody, and evaluate its potential for small-molecule design.

MATERIALS AND METHODS

Peptide Synthesis. All peptides were synthesized as described in the previous paper in this issue (*18*).

Inhibition of VEGF Binding by Peptides. To measure the ability of peptides to inhibit human $VEGF_{8-109}$ binding to KDR, ELISA plates were coated with 2 mg/mL rabbit $F(ab')_2$ to human IgG Fc (Jackson ImmunoResearch, West Grove, PA) in 50 mM carbonate buffer, pH 9.6, at 4 °C overnight and blocked with PBS-0.5% BSA at room temperature for 1 h. Diluted conditioned medium containing 0.2 mg/mL of human KDR(1−7)−IgG (*19*) in PBS−0.5% BSA and 0.05% polysorbate 20 was incubated on the plate for 1 h. Standards (0.16−168 nM $VEGF_{8-109}$ in monomer) and 2-fold serial dilutions of peptides were incubated with 10 nM biotinylated $VEGF_{8-109}$ for 2 h in tubes. The solutions from the tubes were then transferred to the ELISA plates and incubated for 1 h. Bound biotinylated $VEGF_{8-109}$ was detected using peroxidase-labeled streptavidin (Sigma, Saint Louis, MO) followed by 3,3′,5,5′-tetramethyl benzidine (Kirkegaard & Perry Laboratories, Gaithersburg, MD) as the substrate. Plates were washed between steps. Absorbance was read at 450 nm on a V_{max} plate reader (Molecular Devices, Menlo Park, CA). Titration curves were fit with a four-parameter nonlinear regression curve-fitting program (KaleidaGraph, Synergy software, Reading, PA). Concentrations of peptides corresponding to the midpoint absorbance of the titration curve of the standard were calculated and used as the IC_{50} values. Because of differences in assay conditions, the ELISA generally gave IC_{50} values approximately 4-fold higher than those obtained by BIAcore (*18*), otherwise, the results obtained with the two assays were consistent.

NMR Spectroscopy. All NMR spectra were acquired at 35 °C on a Bruker AMX-500 spectrometer. The sample of the complex between peptide v108 and VEGF11−109 was made by addition of 50 μL of 7.2 mM v108 solution to 450 μL of 0.4 mM $VEGF_{11-109}$ (dimer) to give final concentrations of 0.72 and 0.36 mM for the peptide and protein, respectively (*18*). Protein and peptide concentrations were determined spectrophotometrically using estimated molar extinction coefficients of ϵ_{280} = 11 280 and 7 090, respectively.

Crystallization and Data Collection. Human $VEGF_{8-109}$ was expressed, refolded, and purified as described previously (*20*), then concentrated to 20 mg/mL in 0.1 M NaCl with 20 mM TRIS−HCl, pH 7.5. Lyophilized peptide was dissolved at a concentration of 1.5 mM and mixed in 10% molar excess with VEGF, resulting in an 11 mg/mL solution of the VEGF:peptide complex. Crystals were grown at room temperature by vapor diffusion in hanging drops. The droplets contained a mixture of 2 μL of complex solution and 2 μL of reservoir solution [30% poly(ethylene glycol)-4000, 0.2 M ammonium sulfate, and 0.1 M sodium acetate, pH 5]. The resulting crystals reached their maximum size of 75 × 75 × 120 μm in about 1 week. They belong to space group $P2_12_12_1$ and have cell dimensions of a = 47.7 Å, b = 74.6 Å, and c = 79.9 Å. A crystal was flash-frozen in liquid nitrogen after dipping it into reservoir solution containing 20% glycerol and used to collect a complete data set to 1.9 Å resolution on beam line 7-1 at the Stanford Synchrotron Radiation Laboratory (λ = 1.08 Å) equipped with an imaging plate scanner (MAR-research). The data were processed using DENZO and SCALEPACK (*21*), producing 23 253 unique reflections (redundancy 5.1) with an $R_{merge}(I)$ of 4.5% and an overall completeness of 99.6%.

Structure Determination and Refinement. The structure was solved by molecular replacement using program AMoRe (*22*) and a VEGF monomer taken from the high-resolution structure of VEGF in complex with domain-2 of the Flt-1 receptor (*12*). Using all reflections between 12 and 4 Å and an integration sphere from 4 to 25 Å did not result in a prominent peak in the rotation function. However, after translation search and rigid body refinement with the top 10 peaks of the rotation search, the correct solution had a correlation coefficient of 26.9% and an R-value of 52.6% (next peak: correlation coefficient, 23.7%; R-value, 53.0%). This solution was fixed, and the subsequent translation search for the second monomer resulted in a clear solution with a correlation coefficient of 30.0% and an R-value of 51.1% (next peak: correlation coefficient, 20.1%; R-value, 54.6%). Inspection of both solutions with program O (*23*) revealed that the monomers formed the expected dimer. Rigid body refinement of both VEGF monomers further decreased the R-value to 46.6% and increased the correlation coefficient to 40.7%. Before further refinement, 6% of the reflections was sequestered for monitoring of the free R-value (*24*). After an initial simulated annealing refinement with program X-PLOR (*25*), the free R-value dropped to 43.0% for all reflections in the resolution range between 8.0 and 2.0 Å. At this stage, the $2F_o - F_c$ map showed clear electron density for most of both peptide molecules, and residues 3−16 of each molecule were built into this map. Subsequent refinement was done with program REFMAC (*22*), using all reflections between 20 and 1.9 Å and alternating with rounds of model building using program O. After placing water molecules using program ARP (*22*), the R-value reached its final value of 19.0% (with a free R-value of 27.3%).

RESULTS

NMR Studies. Initial NMR data acquired for the free peptide v108 at pH 5.6 and 10 °C showed that the peptide does not adopt a preferred conformation in solution (*18*). Comparison of ^1H-^{15}N HSQC spectra of free and peptide-complexed $VEGF_{11-109}$, at both 35 and 45 °C, allowed the identification of the peptide-binding site on the surface of VEGF (*18*). The perturbed residues (*16−18*, 21, 36−39, 41−48, 77−84, 86, 90, and 92−97) were found to cluster at the poles of the VEGF dimer and include residues previously identified as being involved in receptor binding (*9*, *11*).

Comparison of 1D ^1H NMR spectra of the free peptide and the free protein with the spectrum obtained from the complex provides further information on how the peptide interacts with the protein in solution. For instance, Figure 1A shows that the resonance corresponding to Trp_P3 $^1H\epsilon1$ in the peptide is broadened beyond detection in the complex, suggesting that the tryptophan side chain may be involved

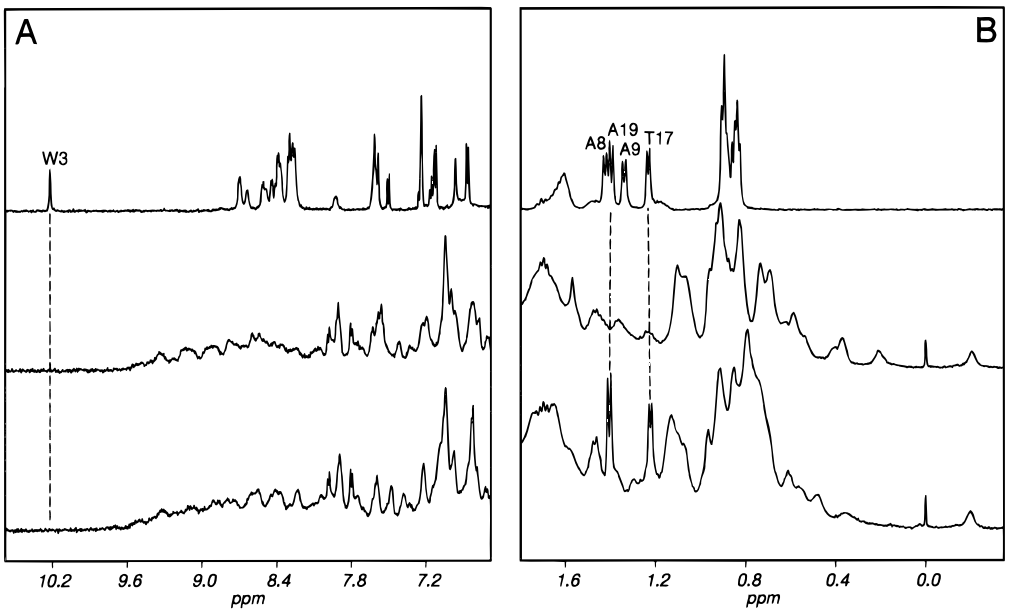

FIGURE 1: 1D ^{1}H NMR spectra of free peptide v108 at pH 5.6 (top), free ^{15}N-labeled $VEGF_{11-109}$ (pH 7.0) (middle), and complex (pH 7.0) (bottom). (A) Amide and aromatic and (B) methyl regions. Complex was formed from an approximately stoichiometric mixture (2 peptide:1 protein dimer) of v108 and ^{15}N-labeled $VEGF_{11-109}$. Note that the protein amide protons were not decoupled from their attached ^{15}N nuclei in these experiments.

Table 1: Crystallographic Refinement and Model Statistics

Model	
total number of residues	224
missing residues	
VEGF-I	8−12, 109
VEGF-II	8−12, 37−42, 109
Pep-I	none
Pep-II	19−20
total number of non-H atoms	2186
no. of water molecules	383
avg *B*-factors (Å^2)	
VEGF-I	24.2
VEGF-II	23.7
Pep-I	26.0
Pep-II	28.4
Diffraction Agreement	
resolution (Å)	20.0−1.9
R-value ($F > 0$)	0.190
no. of reflections	21 270
free *R*-value ($F > 0$)	0.273
no. of reflections	1345
Stereochemistry	
rms difference in bond distances (Å)	0.012
rms difference in bond angles (deg)	2.50
rms ΔB of bonded atoms (Å^2)	1.9

in a conformational exchange process. On the other hand, the methyl resonances of Thr_P17 and Ala_P19 remain sharp upon binding to VEGF (Figure 1B), suggesting that the C-terminal region of the peptide does not interact significantly with the protein. More detailed analysis of the conformation of the complex in solution was not possible, due mainly to the significant aggregation observed previously for the free protein (*26*); the aggregation state of the protein did not change significantly upon peptide binding.

Quality of the Crystal Structure. The structure of the complex between peptide v108 and $VEGF_{8-109}$ was refined to an *R*-value of 19.0% (free *R*-value 27.3%) using all reflections between 20 and 1.9 Å resolution (Table 1). The crystallographic asymmetric unit contains one homodimeric VEGF molecule with a 20-mer peptide molecule bound at either pole of the dimer; these two crystallographically independent peptide molecules will be denoted Pep-I and Pep-II. The stereochemical parameters of the refined model are good (Table 1) with 92.0% of all nonglycine residues located in the "most favorable" (*27*) and all other nonglycine residues located in the "additionally allowed" regions of the Ramachandran plot. Of each VEGF monomer, the N-terminal residues 8−12 as well as the C-terminal residue 109 are disordered. Residues 37−42 are well-defined in one monomer (VEGF-I) but are disordered in the second (VEGF-II). All atoms of one of the peptide molecules (Pep-I) have clearly defined electron density, whereas in the other peptide (Pep-II) the two C-terminal residues are disordered.

Structure of Bound Peptide v108. Despite the internal disulfide bridge between Cys_P7 and Cys_P15, the peptide binds in a rather extended conformation, as evidenced by a linear distance of 35 Å between the N- and C-terminus of Pep-I. The two peptide molecules have very similar conformations in their central region (Figure 2), with rms deviations of less than 0.8 Å for the 97 atoms of residues 4−16. In contrast, they differ significantly at their termini, giving rise to a relatively large rms deviation of 1.9 Å for all common 18 Cα atoms. With the exception of Ile_P6, the main-chain torsion angles of residues 1−9 lie in the β-region of the Ramachandran plot, resulting in an almost fully extended conformation of the N-terminal half of the peptide. The residues between the cysteines ($Ala_P8-Ala_P9-Asp_P10-Asp_P11-Tyr_P12-Gly_P13-Arg_P14$) form a type I β-hairpin loop (*28*) with a bulge at Gly_P13. This loop conformation is stabilized by the disulfide bridge as well as three main-chain hydrogen bonds. In addition, the carboxylate moiety of Asp_P10, which is positioned at the tip of the loop, forms hydrogen bonds to the amides of residues 12, 13, and 14 as well as a salt bridge to the side chain of Arg_P14 (Figure 2). Residues 13−18 again adopt an extended conformation (residues 19 and 20 are disordered and presumed flexible in Pep-II), with the side

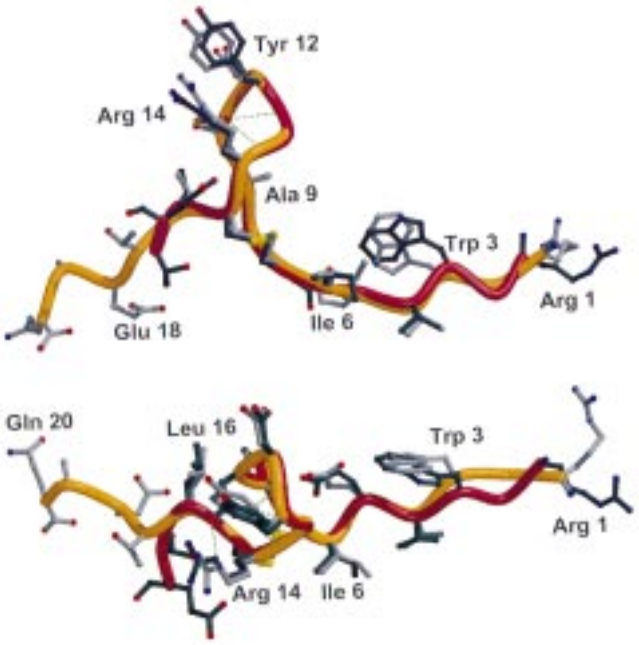

FIGURE 2: Superposition of Pep-I and Pep-II based on the Cα positions of residues 4−16, in two orientations related by a rotation of 90° about the horizontal axis. The main chain is shown in tube representation, with Pep-I depicted in yellow and light gray and Pep-II in red and dark gray. The dotted lines represent the hydrogen-bonds of Asp$_P$10. Selected residues are labeled. Figures 2, 3, 5, and 6 were generated using programs MOLSCRIPT-II (33) and RASTER-3D (34).

chain of Leu$_P$16 forming a mini hydrophobic core by packing against Ala$_P$8, Ala$_P$9, and Asp$_P$10.

VEGF:Peptide Contacts. The peptide is bound to VEGF through interactions mediated by its N-terminal half and the residues in the hairpin loop, while the C-terminal five residues do not contact the protein at all (Figures 3 and 4). The two N-terminal residues interact with the side of VEGF facing the membrane when bound to the Flt-1 receptor (*12*). Residues 3−8 have a slightly irregular β-strand conformation and form six main-chain to main-chain hydrogen bonds to strand β6 of VEGF, adding a fourth strand to the existing antiparallel β-sheet of the growth factor (Figure 5). The backbone of residues 8−10 loops across strand β6 to the opposite face of the VEGF dimer, bringing the peptide hairpin loop into the vicinity of strand β5 of VEGF-I and the N-terminal helix of the other monomer. The peptide residues following the hairpin loop point away from the growth factor and are involved in crystal-packing interactions that are different for Pep-I and Pep-II.

Interface I, the contact area between Pep-I and the VEGF dimer, buries a total of about 1350 Å^2 of solvent-accessible surface, of which over 95% is due to interactions between Pep-I and VEGF-I. Most of the contacts involve residues 89−95 of strand β6 of VEGF-I, whose accessible surface is decreased by 373 Å^2, or 60% of the total VEGF surface buried in this interface. Additional contributions to the buried surface come from residues 79−82 (strand β5) and residues 38−42 in the α2 region, which each contribute about 17% of the buried surface, as well as residue 48 on strand β2. The only amino acid of VEGF-II in van der Waals distance to Pep-I is Phe17, which is located at the N-terminus of helix α1. In interface II, the α2 region of VEGF-II is disordered, resulting in a total calculated buried surface about 200 Å^2 smaller than in interface I.

Pep-I and Pep-II are in contact with a total of 18 and 16 VEGF residues, respectively. However, only the interactions involving Gln89 to Glu93 of VEGF are strictly identical in both interfaces. These are the VEGF residues that form strand β6 and account for all nine hydrogen bonds that are conserved in both interfaces. Six of these are between main-chain atoms and stabilize the formation of the additional β-strand formed by the peptide. Two hydrogen bonds are formed between the side chain of Gln89 and Ala$_P$9−O and Asp$_P$11−Oδ1, and one charged interaction links the side chains of His90 and Glu$_P$5. For both peptide molecules, a substantial contribution to the buried surface is made by Trp$_P$3, but the precise interactions observed differ between the two interfaces (Figure 6). The indole ring is buried deeply in a pocket constituted in part by residues of VEGF and in part by atoms of the peptide itself. This pocket is conserved between the two interfaces, but the conformation of the Trp$_P$3 side chain differs with $\chi 2 = 90°$ in one and $\chi 2 = -90°$ in the other peptide. In Pep-I, the indole ring stacks closely against the guanidinium group of Arg82, and the Nϵ atom is in proximity of the carboxylate of Glu$_P$5 and forms an intramolecular hydrogen bond (Figure 6A). In Pep-II, the stacking interaction appears to be weakened, and the Nϵ is close to the main-chain oxygen of Ile80, enabling formation of an intermolecular hydrogen bond (Figure 6B). The conformational change of the tryptophan side chain is accompanied by small movements of the VEGF residues lining the pocket as well as a difference in the orientation of the side chain of Glu$_P$5. Finally, Tyr39 and Asp41 of VEGF-I are involved in an additional four hydrogen bonds/salt bridges to the N-terminal two residues of Pep-I. Segment 37−42 is disordered in VEGF-II, and the N-terminus of Pep-II adopts a different conformation, interacting with the C-terminal residue of a symmetry related molecule of Pep-I.

Crystal Packing. Each complex interacts with a total of eight symmetry-related complexes, resulting in four different crystal packing environments. Remarkably, the largest of these contact areas buries more than 2000 Å^2 of solvent accessible surface and involves 14 hydrogen bonds. The C-terminal half of Pep-I is responsible for about 50% of the buried surface area and for 11 of the hydrogen bonds. It is inserted like a wedge between strand β5 of VEGF-II and central strands β1 and β3 from both monomers of a symmetry-related VEGF dimer, opening up the entire molecule. Residues Tyr$_P$12 and Arg$_P$14 form four and residues 17−20 form five hydrogen bonds to the two symmetry related VEGF monomers, respectively. In addition, Gln$_P$20 is involved in two hydrogen bonds with the N-terminal arginine of a symmetry related Pep-II molecule. This crystal contact is likely responsible for the disruption of helix α2 of VEGF-II, since the position of the symmetry related C-terminus of Pep-I is sterically incompatible with that of helix α2.

Comparison to Other VEGF Structures. Ten crystallographically independent monomers of VEGF have been reported that are defined by crystal structures with a resolution of better than 2 Å (*8*, *12*); in addition, a complex with a Fab fragment is known to 2.4 Å resolution (*13*). All of these structures superimpose well, with rms deviations between 0.3 and 0.9 Å for 94 Cα atoms, the largest movements occurring at the tip of the loops connecting strands

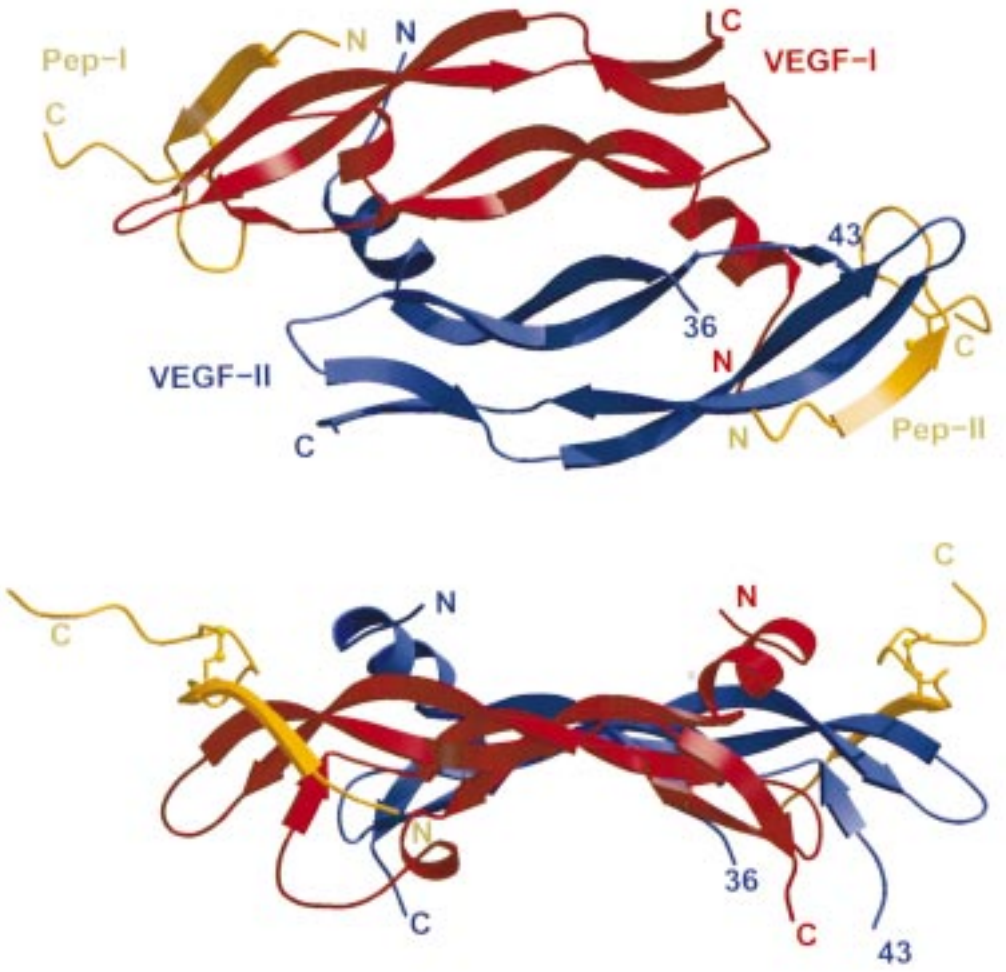

FIGURE 3: Ribbon representation of the complex between $VEGF_{8-109}$ and peptide v108 in two orientations, related by a rotation of 90° about the horizontal axis. The two VEGF monomers−I and −II are shown in red and blue, respectively, with the peptide molecules v108 bound at both poles of the VEGF dimer in yellow. All termini are labeled and disulfide bonds are shown in ball-and-stick drawings.

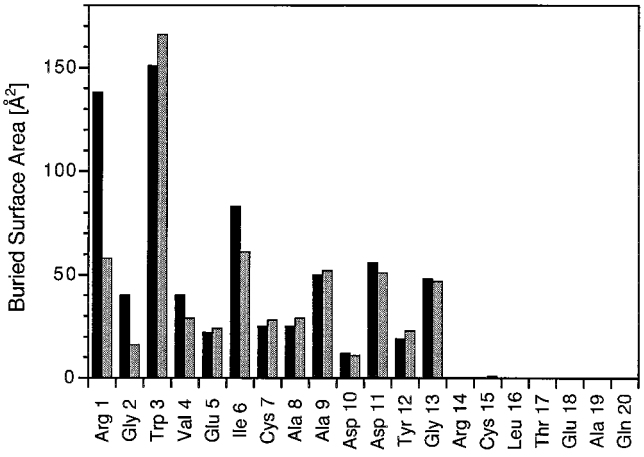

FIGURE 4: Surface area (Å²) of peptide residues buried in the interface with VEGF. Black bar, Pep-I; shaded bar, Pep-II. The peptide sequence and residue numbering are shown at the *x*-axis.

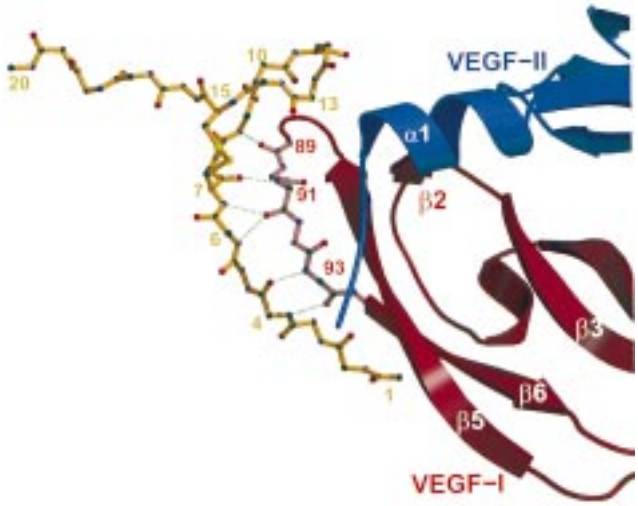

FIGURE 5: Main-chain hydrogen bonds in interface-I. The molecules are colored according to Figure 3. All main-chain atoms and the disulfide bridge of Pep-I as well as residues 89−93 of VEGF-I are shown in ball-and-stick representation.

β3 to β4 and β5 to β6. It is noteworthy that these 12 structures include eight copies of the free monomer as well as four monomers taken from the complex with the second domain of the Flt-1 receptor or the Fab fragment; thus, receptor or antibody binding does not impose major conformational changes on VEGF. The two VEGF monomers from the peptide complex are similar to each other (0.85 Å for 88 common Cα positions), but unexpectedly differ significantly from all previous structures. Monomer I has rms deviations to the earlier structures of 0.85−1.27 Å (94 Cαs); monomer II is even more different with rms deviations

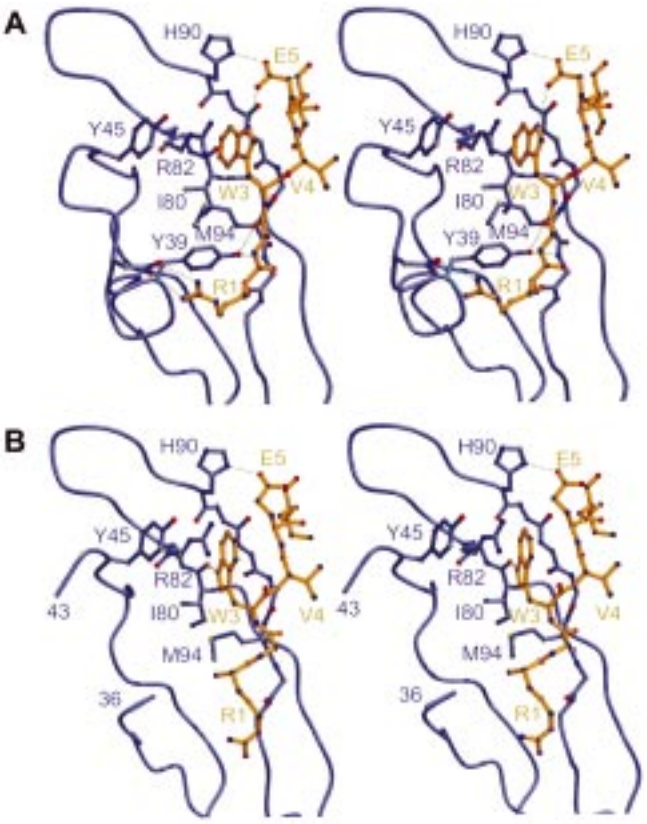

FIGURE 6: Stereoview showing the environment of Trp_P3 in the complex between peptide v108 and VEGF. The peptides are depicted in yellow, the main chain of VEGF is shown in tube representation with selected side chains in blue. All nonconserved hydrogen bonds of the two interfaces are shown in dotted lines. (A) Interface-I; (B) interface-II (note that segment 37−42 of VEGF-II is disordered).

between 1.30 and 1.81 Å (88 Cα positions). In contrast to the previous VEGF structures, the differences are not restricted to the loop regions but affect the entire VEGF dimer. The most obvious change occurs in the α2 region of VEGF-II, where no electron density is observed for residues 37−42. Overall, the changes can be described as a flattening of the shape of the VEGF dimer compared to previous structures. This is not the result of a single hinge movement or shear motion but rather a consequence of many concerted changes distributed throughout the molecule. We believe these changes are induced by the unusually large crystal contact described above rather than a direct effect of peptide binding [the NMR data do not support global structural changes in solution (*18*)].

Truncation Studies of the Peptide. Solution studies and the crystal structure of the v108:VEGF complex show that the four C-terminal residues of the peptide are not in contact with VEGF and suggest that they are unnecessary for binding. As expected, deletion of these residues from peptide v108 had very little effect on peptide IC_{50} values (8.2 μM for v108 vs 20 μM for v113, Table 2). The crystal structure of the complex showed that the seven N-terminal residues of the peptide (RGWVEIC) bind to VEGF in an extended conformation and appear to contribute the most significant contacts. We therefore tested whether the truncated peptide $RGWVEIA\text{-}NH_2$ (v110) could inhibit VEGF binding to KDR in an ELISA (Materials and Methods). We also tested the disulfide-cyclized portion ($Ac\text{-}CAADDYGRCL\text{-}NH_2$, v112).

Table 2: Peptide Truncations

Peptide		IC_{50} (μM)	highest assay concentration (μM)
v108	RGWVEICAADDYGRCLTEAQ-NH_2	8.2[a]	
v113	RGWVEICAADDYGRCL-NH_2	20	150
v110	RGWVEIA-NH_2	nd[b]	400
v112	Ac-CAADDYGRCL-NH_2	nd	700
v120	Ac-GWVEICAADDYGRCL-NH_2	83	400
v121	Ac-WVEICAADDYGRCL-NH_2	130	150
v122	Ac-VEICAADDYGRCL-NH_2	nd	190
v123	Ac-EICAADDYGRCL-NH_2	nd	1000
v124	Ac-ICAADDYGRCL-NH_2	nd	1000

[a] ELISA measurements for all peptides except v108 were performed in parallel as described in the Materials and Methods. Control IC_{50} values for $VEGF_{8-109}$ agreed well for the two assay runs (1.5 and 1.6 nM monomer concentration). IC_{50} values in the ELISA are generally 4-fold higher than those reported in the previous paper in this issue (see the Materials and Methods in ref 18). [b] Not detectable.

No inhibition could be observed with either fragment, even at relatively high peptide concentrations (Table 2). Hummel−Dreyer chromatography (*29*) confirmed that neither peptide bound to VEGF without blocking the receptor interaction surface (not shown). Therefore, both the disulfide loop and the extended N-terminal segment contribute significantly to the binding affinity of the peptide.

We then N-terminally truncated peptide v113 one residue at a time to see whether any of these shorter peptides could inhibit VEGF binding to receptor (Table 2). The peptide lacking Arg_P1 (v120) had an IC_{50} of 83 μM, while further deletion of Gly_P2 (v121) only slightly increased the IC_{50} to 130 μM. This inhibition by v121 was clearly detectable (20%) at 6 μM peptide (not shown). In contrast, no inhibition was observed for peptide v122 up to the highest concentration tested (190 μM), demonstrating that deletion of Trp_P3 results in a greater than 30-fold loss in binding affinty.

DISCUSSION

Peptide Binding. In the crystal structure of the complex, residues 17−20 of each of the two independent peptide molecules extend away from VEGF (these residues form a crystal packing interaction for Pep-I, while residues 19 and 20 of Pep-II are disordered). This is not a crystal-packing artifact, because our NMR experiments show that the methyl resonances of Thr_P17 and Ala_P19 remained sharp upon binding protein, suggesting that the C-terminal region of the peptide does not interact significantly with the protein in solution either. In light of these observations, we tested the binding affinity of peptides truncated at the C-terminus. The results showed that residues $Thr_P17-Glu_P18-Ala_P19-Gln_P20$ could be deleted with only an about 2-fold decrease in binding affinity. In contrast, Leu_P16 is important for affinity, because mutation to alanine abolished all measurable binding (data not shown), even though its side chain is not in contact with VEGF. This observation suggests that the small hydrophobic core consisting of Leu_P16, Ala_P8, Ala_P9, and Asp_P10 is important for stabilizing the bound conformation of the peptide.

The first three residues of the peptide contribute a large fraction (40−46%) of the total buried surface area of the peptide, but the detailed interactions of these residues with VEGF differ significantly between Pep-I and Pep-II. For example, Arg_P1 of Pep-I makes three hydrogen bonds to VEGF, whereas Arg_P1 of Pep-II interacts with a symmetry related Pep-I molecule. For Trp_P3, the crystal structure shows different conformations for the side chain in the two peptide molecules, although it is deeply buried in the interface in both cases. These results are consistent with the results of the NMR experiments which suggested that the tryptophan side chain is involved in a conformational exchange process in solution. To investigate the importance of the N-terminal residues for VEGF binding, the binding affinities of several N-terminally truncated peptides were measured. Truncation of Arg_P1 increased the IC_{50} by only about 4-fold, and deletion of one more residue increased the IC_{50} by only another 2−3-fold. In contrast, truncation of Arg_P1-Trp_P3 in v108, as well as substitution of Trp_P3 with alanine in a closely related peptide (data not shown), abolished binding. Therefore, the specific, albeit nonconserved, interactions observed for the side chain of Trp_P3 contribute significantly to the total binding energy, while the N-terminal two residues are not essential for VEGF binding. The moderate decrease in binding affinity observed upon deletion of Arg_P1 and Gly_P2 most likely reflects the decrease in buried surface caused by the loss of the nonspecific interactions made by these residues.

Attempts at improving the affinity of the v108 peptide resulted in an only slightly tighter-binding version with four changes, all in the peptide core, namely $Ala_P8 \rightarrow$ Glu, $Ala_P9 \rightarrow$ Ser, $Asp_P11 \rightarrow$ Val, and $Tyr_P12 \rightarrow$ Trp (peptide v128a in Table 1 of ref *18*). Inspection of the structure of the v108:VEGF complex suggests that introduction of a serine side chain at position 9 may add a favorable interaction with His90 of VEGF. For the remaining changes, new favorable interactions appear unlikely. Alanine-scanning mutagenesis (*30*) of the peptide core region of this peptide identified three residues as critical for binding affinity (data not shown). Two of these, Asp_P10 and Leu_P16, appear to be important for stabilizing the bound conformation of the peptide; the side chain of only the third, Ile_P6, is in the interface with VEGF.

Given the binding mode of v108, with much of the binding energy apparently derived from main-chain to main-chain interactions, it is not surprising that attempts to increase binding affinity by further sequence randomization have been largely unsuccessful. All but one of the side chains in the disulfide loop point away from the target, making it nearly impossible to introduce new favorable interactions by side-chain substitutions. In fact, only three of the side chains in the entire peptide have significant contacts to VEGF, and of these three, only Trp_P3 and Ile_P6 are important affinity determinants. In terms of small molecule design, peptide v108 is clearly a poor lead molecule. The extended binding mode does not bode well for small-molecule mimics, and the scarcity of specific side-chain-mediated interactions provides little basis for structure-based design. Therefore, in light of the structural information we have obtained for the bound state of v108, this peptide is a far inferior candidate for minimization approaches than peptides that are inherently structured in solution, such as those that have been selected for blocking the interaction between insulin-like growth factor-1 and its binding protein-1 (*31*).

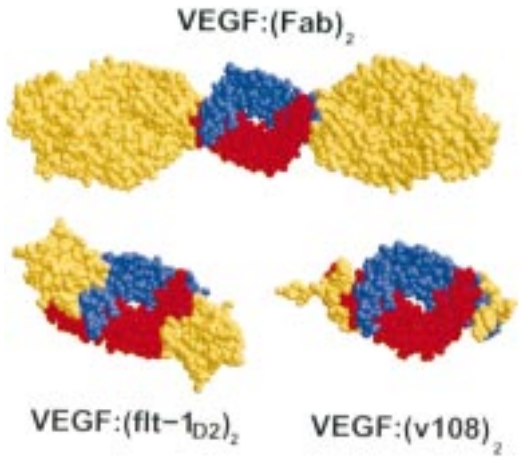

FIGURE 7: Space filling models of VEGF in complex with the Fab fragment of a neutralizing antibody (top), the second domain of the Flt-1 receptor (bottom left) and peptide v108 (bottom right), as seen in different crystal structures. The VEGF monomers are depicted in red and blue, respectively, with the bound ligands in yellow. All complexes are shown in approximately the same orientation. This figure was generated using program CONIC (35).

Receptor vs Antagonist Binding: Two Distinct Binding Modes. Over the past two years, a wealth of structural and functional information has been developed on the interaction of VEGF both with its receptors and with receptor antagonists (*9*, *11*−*13*, *32*). The receptor-binding face of VEGF, as observed in the complex with domain 2 of Flt-1 (Flt-1D2) and deduced from mutagenesis data for KDR and Flt-1, is located at the poles of the homodimer. In the complex with Flt-1D2, both VEGF monomers contribute to the total buried surface of 1600 Å^2 in a ratio of about 65/35% (*12*). In contrast, a receptor-blocking Fab fragment, while burying an equally extensive area (about 1750 Å^2) of VEGF, binds almost exclusively to segment $\beta5-\beta6$ of monomer 1 (*13*). In its extensive interaction with strand $\beta6$ of VEGF, binding of peptide v108 is more similar to that of the Fab fragment than that of the receptor (Figure 7). Only 5 out of the 13 VEGF residues in the interface with v108 are in contact with Flt-1D2 in the receptor complex, compared to 12 of 13 in the complex with the Fab. The nature of the interactions observed is also similar between peptide and Fab complexes and distinct from those seen in the receptor complex. The receptor interface is dominated by hydrophobic interactions with only two intermolecular hydrogen bonds in the entire contact area. In contrast, 15 intermolecular hydrogen bonds are present in the interface of the peptide complex and 10 in the Fab complex, indicating that hydrophilic interactions are important in each of these cases. Furthermore, all VEGF atoms involved in conserved hydrogen bonds in the peptide complex also form hydrogen bonds to the Fab fragment. Some of the interactions show a large degree of conservation: five main-chain atoms from segment Gln89 to Glu93 of VEGF form hydrogen bonds to main-chain atoms in both the peptide and the antibody complex, and the carbonyl oxygen of Ile80 hydrogen bonds to a buried aromatic side chain occupying the same position in each complex (Trp_P3 of the peptide II or Tyr102 of the Fab). It is interesting to note that the other two classes of receptor-blocking peptides we have identified (*18*) appear to bind in a different manner than peptide v108, possibly in a mode resembling more that of the receptor. The ability of these phage-derived peptides

to achieve diverse modes of binding, resembling those of the natural protein partners, underscores the versatility of naive peptide phage display in targeting relevant binding sites on protein surfaces.

ACKNOWLEDGMENT

We thank the staff at SSRL for help with beam line 7-1 and Jim Wells for numerous scientific discussions and support.

REFERENCES

1. Ferrara, N., and Davis-Smyth, T. (1997) *Endocrine Rev. 18*, 4−25.
2. Vaisman, N., Gospodarowicz, D., and Neufeld, G. (1990) *J. Biol. Chem. 265*, 19461−19466.
3. Ferrara, N. (1995) *Breast Cancer Res. Treat. 36*, 127−137.
4. Folkman, J. (1995) *Nat. Med. 1*, 27−31.
5. Kim, K. J., Li, B., Winer, J., Armanini, M., Gillet, N., Phillips, H. S., and Ferrara, N. (1993) *Nature 362*, 841−844.
6. Presta, L. G, Chen, H., O′Connor, S. J., Chisholm, V., Meng, Y. G., Krummen, L., Winkler, M., and Ferrara, N. (1997) *Cancer Res. 47*, 4593−4599.
7. Baca, M., Presta, L. G., O'Connor, S. J., and Wells, J. A. (1997) *J. Biol. Chem. 272*, 10678−10684.
8. Muller, Y. A., Christinger, H. W., Keyt, B. A., and de Vos, A. M. (1997) *Structure 5*, 1325−1338.
9. Muller, Y. A., Li, B., Christinger, H. W., Wells, J. A., Cunningham, B. C., and de Vos, A. M. (1997) *Proc. Natl. Acad. Sci. U.S.A. 94*, 7192−7197.
10. Sun, P. D., and Davies, D. R. (1995) *Annu. Rev. Biophys. Biomol. Struct. 24*, 269−291.
11. Keyt, B. A., Nguyen, H. V., Berleau, L. T., Duarte, C. M., Park, J., Chen, H., and Ferrara, N. (1996) *J. Biol. Chem. 271*, 5638−5646.
12. Wiesmann, C., Fuh, G., Christinger, H. W., Eigenbrot, C., Wells, J. A., and de Vos, A. M. (1997) *Cell 91*, 695−704.
13. Muller, Y. A., Chen, Y., Christinger, H. W., Li, B., Cunningham, B. C., Lowman, H. B., and de Vos, A. M. (1998) *Structure 6*, 1153−1167.
14. James, G. L., Goldstein, J. L., Brown, M. S., Rawson, T. E., Somers, T. C., McDowell, R. S., Crowley, C. W., Lucas, B. K., Levinson, A. D., and Marsters, J. C., Jr. (1993) *Science 260*, 1937−1942.
15. McDowell, R. S., Gadek, T. R., Barker, P. L., Burdick, D. J., Chan, K. S., Quan, C. L., Skelton, N., Struble, M., Thorsett, E. D., Tischler, M., Tom, J. Y. K., Webb, T. R., and Burnier, J. P. (1994) *J. Am. Chem. Soc. 116*, 5069−5076.
16. McDowell, R. S., Blackburn, B. K., Gadek, T. R., McGee, L. R., Rawson, T., Reynolds, M. E., Robarge, K. D., Somers, T. C., Thorsett, E. D., Tischler, M., Webb, R. R., II, and Venuti, M. C. (1994) *J. Am. Chem. Soc. 116*, 5077−5083.
17. McDowell, R. S., Elias, K. A., Stanley, M. S., Burdick, D. J., Burnier, J. P., Chan, K. S., Fairbrother, W. J., Hammonds, R. G., Ingle, G. S., Jacobsen, N. E., Mortensen, D. L., Rawson, T. E., Won, W. B., Clark, R. G., and Somers, T. C. (1995) *Proc. Natl. Acad. Sci. U.S.A. 92*, 11165−11169.
18. Fairbrother, W. J., Christinger, H. W., Cochran, A. G., Fuh, G., Keenan, C. J., Quan, C., Shriver, S. K., Tom, J. Y. K., Wells, J. A., and Cunningham B. C. (1998) *Biochemistry 38*, 17754−17764.
19. Park, J. E., Chen, H., Winer, J., Houck, K. A., and Ferrara, N. (1994) *J. Biol. Chem. 269*, 75646−75654.
20. Christinger, H. W., Muller, Y. A., Berleau, L. T., Keyt, B. A., Cunningham, B. C., Ferrara, N., and de Vos, A. M. (1996) *Proteins 26*, 353−357.
21. Otwinowski, Z., and Minor, W. (1997) *Methods Enzymol. 276*, 307−326.
22. CCP4 (1994) *Acta Crystallogr., Sect. D 50*, 760−763.
23. Jones, T. A., Zou, J.-Y., Cowan, S. W., and Kjeldgaard, M. (1991) *Acta Crystallogr., Sect. A 47*, 110−119.
24. Brünger, A. T. (1992) *Nature 355*, 472−475.
25. Brünger, A. T., Krukowski, A., and Erickson, J. W. (1990) *Acta Crystallogr., Sect. A 46*, 585−593.
26. Fairbrother, W. J., Champe, M. A., Christinger, H. W., Keyt, B. A., and Starovasnik, M. A. (1997) *Protein Sci. 6*, 2250−2260.
27. Laskowski, R. A., MacArthur, M. W., Moss, D. S., and Thornton, J. M. (1993) *J. Appl. Crystallogr. 26*, 283−291.
28. Sibanda, B. L., Blundell, T. L., and Thornton, J. M. (1989) *J. Mol. Biol. 206*, 759−777.
29. Hummel, J. P., and Dreyer, W. J. (1962) *Biochim. Biophys. Acta 63*, 530−532.
30. Wells, J. A. (1991) *Methods Enzymol. 202*, 390−411.
31. Lowman, H. B., Chen, Y. M., Skelton, N., J., Mortensen, D. L., Tomlinson, E. E., Sadick, M. D., Robinson, I. C. A. F., and Clark, R. G. (1998) *Biochemistry 37*, 8870−8878.
32. Fuh, G., Li, B., Crowley, C., Cunningham, B. C., and Wells, J. A. (1998) *J. Biol. Chem. 273*, 11197−11204.
33. Kraulis, P. J. (1991) *J. Appl. Crystallogr. 24*, 946−950.
34. Merritt, E. A., and Murphy, M. E. P. (1994) *Acta Crystallogr., Sect. D 50*, 869−873.
35. Huang, C. C., Pettersen, E. F., Klein, T. E., Ferrin, T. E., and Langridge R. (1991) *J. Mol. Graph. 9*, 230−236.

BI9819327